Radiology

Insights into the Epiphyseal Cartilage Origin and Subsequent Osseous Manifestation of Juvenile Osteochondritis Dissecans with a Modified Clinical MR Imaging Protocol: A Pilot Study[1]

Jutta Ellermann, MD, PhD
Casey P. Johnson, PhD
Luning Wang, PhD
Jeffrey A. Macalena, MD
Bradley J. Nelson, MD
Robert F. LaPrade, MD, PhD

© RSNA, 2016

Purpose: To retrospectively determine if a modified clinical magnetic resonance (MR) imaging protocol provides information on the origin of juvenile osteochondritis dissecans (JOCD) lesions and allows for staging on the basis of the proposed natural history of JOCD to better guide clinical management of the disease.

Materials and Methods: This institutional review board–approved, HIPAA-compliant, retrospective study was performed in 13 consecutive patients (mean age, 14.9 years; age range, 10–22 years; nine male and four female patients) and one additional comparative patient (a 44-year-old man), in which 19 knees with 20 JOCD lesions were imaged. Seventeen lesions occurred in the medial femoral condyle, two occurred in the lateral femoral condyle, and one occurred in the medial trochlea. The clinical 3-T MR imaging protocol was supplemented with a routinely available multiecho gradient-recalled-echo sequence with the shortest attainable echo time of approximately 4 msec (T2* mapping).

Results: At the earliest manifestation, the lesion was entirely cartilaginous ($n = 1$). Subsequently, primary cartilaginous lesions within the epiphyseal cartilage developed a rim calcification that originated from normal subjacent bone, which defined a clear cleft between the lesion progeny and the parent bone ($n = 9$). Secondarily, progeny lesions became ossified ($n = 7$) while at the same time forming varying degrees of osseous bridging and/or clefting with the parent bone. Two healed lesions with a linear bony scar and one detached lesion were identified.

Conclusion: The modified MR imaging protocol allowed for identification of the epiphyseal cartilage origin and subsequent stages of ossification in JOCD. The approach allows further elucidation of the natural history of the disease and may better guide clinical management.

©RSNA, 2016

Juvenile osteochondritis dissecans (JOCD) is a common and potentially serious pediatric joint disease, the natural history of which is still not understood (1). The term *osteochondritis dissecans* (OCD) was first used in 1887 (2) to describe the hallmark of the disease: an osteochondral sequestrum progeny separated from the parent bone. However, it is widely acknowledged that little progress has been made in understanding the disease origin or pathogenesis of JOCD since it was first described (1). Furthermore, the American Academy of Orthopedic Surgeons published clinical practice guidelines for the diagnosis and treatment of JOCD on the basis of an expert panel review of the literature (3), and only four of 16 recommendations had strong panel consensus, owing to "absence of reliable evidence." This demonstrates the current lack of fundamental knowledge in the diagnosis and treatment of JOCD in young patients.

Most JOCD studies have been focused on radiographic (4,5), magnetic resonance (MR) imaging (6–8), and arthroscopic (9) classification systems to define the stability of the progeny and parent bone interface, which is then used to make treatment recommendations (10). However, these classification systems do not take into account other contributing factors, namely lesion tissue composition and the specific developmental stage of the lesion, which are important for overall prognosis. Ideally, MR imaging would provide this information, but current clinical imaging protocols cannot be used to unambiguously distinguish lesion composition, which includes osseous, cartilaginous, and calcified regions. This is mainly due to the fact that the echo times (TEs) used are too long—typically 20 and 60–80 msec for proton density–weighted and T2-weighted sequences, respectively. At these TEs, the osseous, calcified, and fibrocartilaginous tissues within the lesion complex will appear hypointense without detectable signal intensity differences between them. One potentially useful method is to acquire an array of images at multiple TEs for T2* mapping by using a gradient-recalled-echo sequence. By using the shortest clinically available TE (approximately 4 msec) for the first image in the array, bone, calcifications, cartilage, and fibrous tissues can be differentiated and characterized despite having short-T2 components.

The purpose of our retrospective study was to determine if a modified clinical MR imaging protocol provides information on the origin of JOCD lesions and allows for staging based on the proposed natural history of JOCD to better guide clinical management of the disease.

Materials and Methods

Study Design and Patient Selection
Our study was approved by the local institutional review board and was performed in accordance with Health Insurance Portability and Accountability Act guidelines. Informed consent was waved by the institutional review board for our retrospective study. Images from 18 clinical MR imaging knee examinations in 13 consecutive patients with known JOCD lesions were reviewed retrospectively. Mean ages ± standard deviations for all 13 participants and the subgroups of nine male and four female participants were 14.9 years ± 3.6, 14.1 years ± 2.7, and 16.8 years ± 5.1, respectively. The study group was selected from a database of 3-T knee MR imaging examinations in patients with JOCD performed at our institution between November 2008

Advances in Knowledge

- Our modified MR imaging technique and proposed classification system for juvenile osteochondritis dissecans (JOCD) may help overcome an inherent limitation of current clinical imaging to allow differentiation between tissues that are otherwise hypointense and indistinguishable on MR images.

- JOCD has been previously defined as a localized process in which a focus of subchondral bone separates from the surrounding parent bone; in our study, a clinical protocol supplemented with an additional 5–6-minute imaging sequence demonstrated epiphyseal cartilage necrosis in the lesion, linking JOCD to failure of the articular-epiphyseal cartilage complex, as is consistent with data from animal research.

Implications for Patient Care

- The information obtained from the additional T2*-weighted gradient-recalled-echo sequence added onto the clinical MR imaging protocol for JOCD can potentially enhance visualization of the tissue composition of the lesion and provide staging on the basis of natural history.

- Our results emphasize the secondary, reparative nature of lesion ossification and support the proposed classification system we introduce on the basis of the natural history of the disease, which calls for a fresh look at evidence-based treatment approaches for JOCD.

Table 1

Typical Imaging Parameters for the Clinical Protocol

Sequence	Field of View (cm)	Matrix	Repetition Time (msec)	TE (msec)	Section Thickness and Gap (mm)
Axial T1-weighted	14 × 14	448 × 314	682	94	3.0, 0.3
Axial T2-weighted fat-saturated	14 × 14	512 × 354	3200	54	3.0, 0.3
Sagittal T2-weighted fat-saturated	14 × 16	384 × 307	5080	60	2.5, 0.25
Sagittal proton density–weighted	14 × 16	512 × 354	3000	10	2.5, 0.25
Coronal T2-weighted fat-saturated	15 × 16	384 × 269	3000	55	3.0, 0.3
Coronal proton density–weighted	15 × 16	384 × 346	3000	40	3.0, 0.3
Three-dimensional double-echo steady-state	15 × 15 × 15	256 × 256 × 256	12.3	4.9	0.6 isotropic, 0
Add-on T2* mapping	15 × 16	384 × 384	1379	4.0, 11.9, 19.4, 27, 34.5, 42, 49	2.0, 0.4

Note.—Parameters varied marginally between studies. Acquisition time was approximately 30 minutes plus 5–6 minutes for T2* mapping.

and December 2015 that included the supplemental T2* mapping sequence, which is the advanced clinical imaging protocol for JOCD at our institution. Inclusion criteria were (a) no prior lesion surgery and (b) JOCD diagnosis based on MR imaging assessment of an open physis (8) or medical records that documented juvenile onset of the disease before age 18. We determined open physis in 10 patients on the basis of MR images and juvenile onset before age 18 in three patients according to medical records. On the basis of these criteria, we also included a comparative 14th participant, a 44-year-old man, who had documented onset of JOCD at age 14 and an event of OCD lesion detachment at age 25, with the respective MR images that demonstrated the defect, which had not been repaired surgically. None of the patients underwent prior lesion surgery. Of the 19 knee MR imaging examinations, five were bilateral knee studies in the same patient, and nine left and 10 right knees with lesions were imaged.

MR Examination

Patients underwent 3-T MR imaging (Siemens Medical Systems, Erlangen, Germany) at our institution by using an eight-channel receive coil or a 15-channel transmit-and-receive knee coil (Siemens Medical Systems). Our standard imaging protocol was supplemented with gradient-recalled-echo–based T2* parametric mapping that added 6 minutes to the acquisition time, as detailed in Table 1. The shortest attainable TE was about 4 msec. The respective image was used to demonstrate contrast between calcified tissues and all other tissues and was displayed with inverted computed tomography (CT)–like image contrast. T2* maps were used to assess the articular-epiphyseal cartilage complex by comparing the lesion with the normal condyle.

MR Imaging Data Analysis

The overall OCD lesion size and location were obtained from the three-dimensional double-echo steady-state images. The largest transverse and anteroposterior dimensions were measured on the coronal and sagittal images, respectively. The maximum depth of the progeny OCD lesion was measured from the articular cartilage surface up to the interface with the parent bone. The interface was not included in the depth measurement of the lesion. The OCD lesion tissue composition was assessed on the basis of the shortest-TE image obtained with the supplemental T2*-weighted gradient-recalled-echo sequence (J.E., a board-certified musculoskeletal radiologist with 8 years of experience). Progeny lesion composition was described as cartilaginous only, cartilaginous with rim calcifications, or ossified.

Classification System

Prior classification systems have been based on the traditional assumption that JOCD has a more or less detached osseous progeny from the underlying parent bone (6). This assumption originates from the fact that JOCD is usually diagnosed late in the course of the disease, at which point lesions are mostly osseous and the overlying articular cartilage is already altered. In contrast, in our study, we considered the preclinical histologic evidence that JOCD occurs subsequent to a focal failure of endochondral ossification (11–15), the process by which growth and/or epiphyseal cartilage is replaced by bone during development of the articular-epiphyseal cartilage complex (16,17). This preclinical cartilaginous form of the disease has been identified consistently in preclinical research in veterinary medicine (18,19) and is rarely recognized in patients, since they first present with symptoms at later stages of the disease. On the basis of our observations in our case series of short-TE images, we classified lesions according to the degree of progressive replacement by mineralization and/or ossification (from minimal to maximal), with additional description of the corresponding interfaces to the parent bone on the basis of the degree of osseous bridging. Specifically, the classifications were as follows: type I, entirely cartilaginous lesion (no cleft at the interface); type II, cartilaginous lesion with complete or incomplete rim calcification (cleft at the interface); type III, partially or completely osseous lesion (varying degrees of osseous bridging and/or clefting at the interface); type IV, healed osseous lesion with a linear bony scar (no cleft at the interface); and
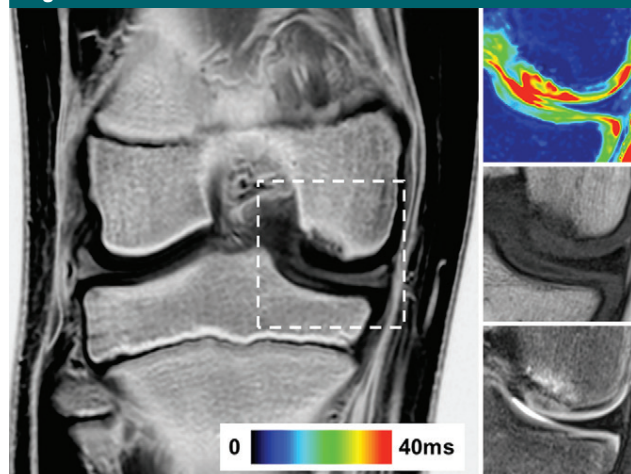
Table 2

Lesion Characteristics as Assessed by Using the Advanced Clinical MR Imaging Protocol

Lesion No.	Patient Age (y)	Patient Sex	Laterality	Location	Lesion Size (mm)*	Type
1	10	Female	Right	MFC	12 × 8 × 15	I
2	11	Male	Right	MFC	11 × 4 × 14	II
3	11	Male	Right	MFC	12 × 6 × 22	II
4	11	Male	Left	MFC	16 × 5 × 20	II
5	12	Male	Right	MFC	12 × 8 × 19	II
6	12	Male	Right	LFC	12 × 5 × 8	II
7	13	Male	Left	MT	17 × 7 × 21	II
8	13	Male	Left	MFC	12 × 7 × 16	II
9	16	Male	Right	MFC	14 × 8 × 29	II
10	19†	Female	Right	MFC	15 × 8 × 19	II
11	12	Female	Left	MFC	17 × 7 × 18	III
12	16	Male	Left	MFC	18 × 6 × 22	III
13	16	Female	Left	LFC	16 × 6 × 21	III
14	16	Male	Left	MFC	11 × 5 × 14	III
15	17	Male	Right	MFC	14 × 8 × 21	III
16	18	Male	Right	MFC	16 × 6 × 12	III
17	22	Female	Right	MFC	15 × 5 × 26	III
18	16	Male	Right	MFC	NA	IV
19	18	Male	Left	MFC	NA	IV
20	25‡	Male	Left	MFC	15 × 6 × 19	V

Note.—Type I = cartilaginous only, type II = cartilaginous with rim calcification, type III = predominately ossified, type IV = healed, type V = detached sequestrum. LFC = lateral femoral condyle, MFC = medial femoral condyle, MT = medial trochlea, NA = not available.

* Size is given in dimensions of transverse dimension × depth × anteroposterior dimension.

† Outlier (patient with delayed skeletal maturation).

‡ Age at the time of the event.

Figure 1

Figure 1: Plot demonstrates the relationship between patient age and lesion type. The proposed natural history of lesion types was found to cluster around age groups. The type II open circle represents an outlier patient with delayed skeletal maturation, and the type V open circle represents a patient whose lesion detached at 25 years of age but who underwent imaging for this study at age 44.

type V, not-healed, detached osseous lesion (sequestrum) (cleft at the interface). All lesion types were determined by reviewing the CT-like shortest-TE MR image. The T2* map was only used to supplement analysis for entirely cartilaginous lesions (type I), in which case we determined whether the epiphyseal cartilage within the lesion was normal or abnormal when compared with the normal condyle of the same knee on the basis of the T2* maps. Abnormality was defined as 2 standard deviations outside of the mean value. Furthermore, the integrity of the overlying articular cartilage was determined for all lesions.

Results

Patient demographics and lesion location, size, and composition are summarized in Table 2. There were a total of 20 OCD lesions, with 17 identified in the MFC, two in the LFC, and one in the medial trochlea. Eighteen knees had one lesion, and one left knee had two lesions (one in the MFC and one in the LFC). There were five patients with bilateral MFC lesions, one of whom also had differing bilateral lesions (one in the MFC and one in the LFC). Overall, there was a narrow range of lesion sizes. All but one of the lesions (lesion 6, in the LFC) were largest in the anteroposterior dimension and shortest in depth, as detailed in Table 2. The information on lesion tissue composition and the relationship between the progeny and the underlying parent bone were combined to introduce the staging system. Interestingly, these lesion types were largely clustered according to age (Fig 1), which suggests a natural progression of lesion development. The staging system is reported next, with observations specific to each lesion type (Figs 2–5).

Type I: Epiphyseal Cartilage Lesion with Necrotic Center (No Cleft at the Interface), Assessed on the Shortest-TE Image and T2* Map

The only type I, entirely cartilaginous lesion was a remnant of epiphyseal cartilage in the youngest patient (10 years of age, Fig 2). The epiphyseal cartilage lesion was thickened and of high intensity, with a hypointense center. The mean T2* value within the lesion measured 40 msec ± 5.9 (vs 24.5 msec ± 3.2 within the other condyle of the same knee), which was abnormal as defined previously. There was not a distinct interface, since the epiphyseal cartilage directly abutted the parent bone. The underlying bone demonstrated a classic concave "shark-bite" appearance, which indicated the focal arrest of the normal endochondral ossification front.

Type II: Epiphyseal Cartilage Lesion with Complete or Incomplete Rim Calcification (Cleft at the Interface), Assessed on the Shortest-TE Image

Nine type II, epiphyseal cartilaginous lesions with a surrounding calcific rim were identified (mean patient age, 13.0

Figure 2

Figure 2: Coronal MR images obtained in a 10-year-old female patient with a type I cartilaginous-only lesion. The CT-like shortest-TE MR image with inverted image contrast (left) demonstrates a focal endochondral ossification defect at the central aspect of the MFC. For comparison, in the area of the lesion (dashed box), a T2* map (top right), proton density–weighted turbo spin-echo image (middle right), and fat-saturated T2-weighted turbo spin-echo image (bottom right) are shown. The T2* map (with relaxation times that correspond to the color bar) demonstrates that that the center of the lesion has T2* values similar to those of the epiphyseal and articular cartilage (green to red). In contrast, the osseous and/or calcified regions of the bone and transition zone have low T2* values (blue). Unlike the T2* map, the standard clinical proton density–weighted and T2-weighted images do not provide a clear depiction of tissue composition.

Figure 3
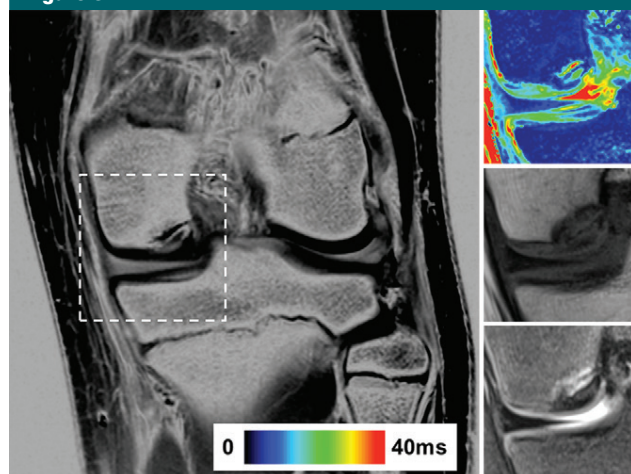
Figure 3: Coronal MR images obtained in a 13-year-old male patient with a type II cartilaginous lesion with a rim calcification that created a fluid-filled cleft. Images are presented as described in Figure 2. The shortest-TE image (left) demonstrates a focal endochondral ossification defect at the MFC. Laminar rim ossification that extends from the periphery toward the notch surrounds and isolates the lesion from the underlying bone, creating a cleft. There is only a thin bridge where the laminar ossification is contiguous with the underlying bone peripherally. The T2* map (top right) demonstrates a cartilaginous lesion center (green) surrounded by calcification (blue). There are high T2* values (red) between the rim calcification and the bone, which is consistent with a fluid-filled cleft. The proton density–weighted image (middle right) provides no clear tissue information. The T2-weighted image (bottom right) shows a small rim of marrow edema and fluid signal intensity at the interface. The lesion itself appears hypointense, without clear delineation of the different tissue components.

Figure 4
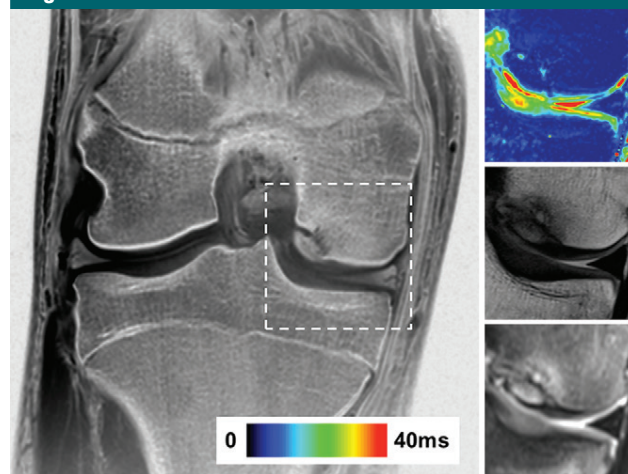
Figure 4: Coronal MR images obtained in a 17-year-old male patient with a type III secondarily ossified lesion with partial cleft and osseous bridging. Images are presented as described in Figure 2. The shortest-TE image (left) demonstrates a focal endochondral ossification defect at the MFC. The entirely ossified lesion is clearly demonstrated. Bridging between underlying bone and lesion is partial, with bridging occurring at more than half of the interface between the parent bone and lesion extending from the peripheral aspect of the lesion. Thin trabeculi traverse the interface, and underlying bone has formed a cortex at the notch, giving the appearance of a hinged sequestrum. The T2* map (top right) demonstrates an osseous lesion (blue) with higher T2* values at the interface. The overlying cartilage is normal, but there are higher-than-normal T2* values in the deep opposing tibial articular cartilage. The proton density–weighted image (middle right) shows the osseous sequestrum but no clear information on the interface. The T2-weighted image (bottom right) demonstrates a focal area of bone marrow edema in underlying bone and sequestrum but also provides no clear information on the interface. Note that on the T2-weighted image, the hyperintensity in the center of the lesion is similar to the signal intensity in the overlying cartilage, even misleadingly suggesting a cartilaginous lesion. The T2* map, in contrast, clearly demonstrates an osseous lesion.

years; age range, 11–16 years; including one outlier 19 years of age who was significantly delayed in skeletal maturation). In these lesions, the rim calcification originated from the normal endochondral ossification front at the periphery of the lesion and appeared first at the parent bone aspect of the lesion, creating a distinct cleft at the interface. The calcific rim then continued to surround the entire epiphyseal cartilage lesion, extending toward the articular side. The core remained largely cartilaginous (Fig 3). Therefore, in general, type II lesions were surrounded by a calcific rim, which likely represents an attempt of repair, and were clearly separated from the parent bone by a cleft.

Type III: Partially or Completely Ossified Lesion (Varying Degrees of Osseous Bridging and/or Clefting at the Interface), Assessed on the Shortest-TE Image

Seven lesions were type III and were thus predominantly osseous as identified on the CT-like shortest-TE MR image (mean patient age, 16.7 years; age range, 12–22 years). The epiphyseal cartilage remnant was ossified. There were varying degrees of new osseous bridging between the lesion and the bone deep to the lesion, leaving a smaller or larger cleft filled with fluid or fibrous tissue that developed a clear linear cortical margination (hinged sequestrum). Images in a 17-year-old male patient (Fig 4) demonstrate the superior CT-like image contrast for bone achieved with short-TE T2*-weighted MR images. Conversely, on the conventional turbo spin-echo images, the lesion appeared to have intermediate image contrast with proton density weighting and was slightly hyperintense on the T2-weighted images, providing no discernable contrast between the lesion and the overlying cartilage.

Type IV: Healed Osseous Lesion with a Linear Bony Scar (No Cleft at the Interface), No Add-On Sequence Needed

Two type IV lesions (Fig 5) that only had a bony scar were observed, which indicated healing of the lesions and complete bridging between the ossified

Figure 5: Coronal proton density–weighted turbo spin-echo MR image obtained in an 18-year-old man with a type IV lesion depicts the hypointense bony scar of a completely healed lesion (arrow).

lesion and the bone deep to the lesion (mean patient age, 17.0 years; age range, 16–18 years).

Type V: Not-Healed Detached Osseous Lesion (Sequestrum), No Add-On Sequence Needed

A type V nonhealed lesion with a detached sequestrum was found in one patient in our case series (25 years old at detachment; 44 years old at imaging).

Since bone and most of the actual OCD lesion appeared hypointense on T2-weighted, T1-weighted, and proton density–weighted clinical turbo spin-echo images, information on tissue composition of the lesion was missing. However, as demonstrated in our case series, the coronal T2*-weighted image obtained with the shortest TE in combination with the quantitative T2* map demonstrated the lesion composition, including whether the lesion was cartilaginous or osseous and whether there was a calcific rim and/or osseous bridging at the interface between the lesion and parent bone. Our observations of five lesion types that occurred

over the progression of JOCD, which formed the basis of our proposed classification system, are summarized in Figure 6.

Discussion

The most important findings of our study were the identification of the early onset of JOCD within the epiphyseal-articular cartilage complex margins and the secondary, reparative nature of lesion ossification, which support a classification based on the natural history of the disease and call for a fresh look at evidence-based treatment approaches to JOCD. By using an imaging sequence with the shortest TE attainable on clinical imaging units, a type I entirely cartilaginous lesion without any osseous components was clearly identified. Subsequently, we observed that lesion types were largely clustered according to age, which suggests a natural progression of JOCD lesion development that leads to the following staging algorithm. During normal development, the epiphyseal cartilage is highly vascularized, and cartilage canals provide
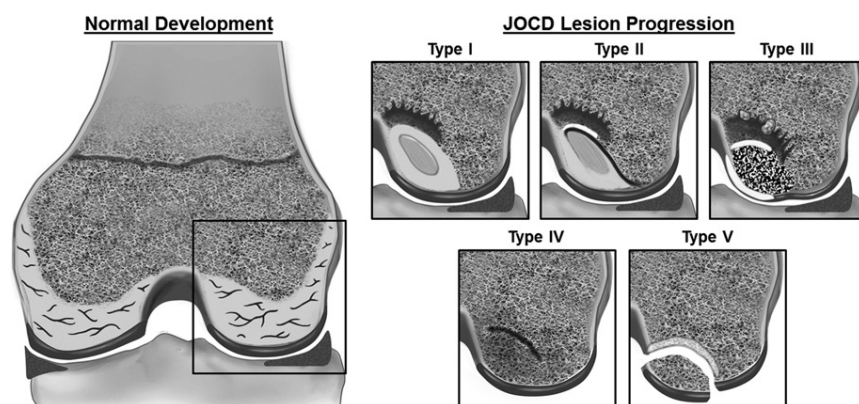
Figure 6

Figure 6: Illustration of the proposed JOCD staging system based on our imaging observations of the natural history of the disease. During normal development, the epiphyseal cartilage is highly vascularized, and cartilage canals provide blood supply to the advancing ossification front while the articular cartilage remains avascular throughout life. There is mounting evidence that focal failure of endochondral ossification and epiphyseal cartilage ischemia will lead to a type I entirely cartilaginous lesion as the earliest disease manifestation. The typical "shark-bite" concave appearance of the parent bone that underlies the type I lesion represents the initial arrest of the advancing ossification front. The process of osseous repair originates from the normal bone next to the lesion with formation of a calcific rim around the lesion (type II), followed by mineralization and subsequent ossification with varying degrees of cleft formation and osseous bridging (type III), which defines lesion stability. At this stage, the lesion might heal (type IV) or become a detached osseous sequestrum (type V).

blood supply to the advancing ossification front (20) while the articular cartilage remains avascular throughout life. There is mounting evidence that focal failure of endochondral ossification and epiphyseal cartilage ischemia will lead to a type I entirely cartilaginous lesion as the earliest disease manifestation, which we identified in the youngest patient in our case series. Although this lesion type was not yet established in human disease, it is widely supported by research on naturally occurring OCD in pigs and horses (18,19,21) and other animal models (11,13,15,22) and confirms that an osseous OCD lesion represents a late-stage finding that results from a reparative process (23) acting on an initial lesion. The typical "shark-bite" concave appearance of the parent bone that underlies the type I lesion represents the initial arrest of the advancing ossification front. The process of osseous repair originates from the normal bone next to the lesion with formation of a calcific rim around the lesion, followed by mineralization and subsequent ossification with varying degrees of cleft formation and

osseous bridging, which defines lesion stability. At this stage, the lesion might heal or become a detached osseous sequestrum.

In vivo information on lesion composition has not previously been available in patients. For cartilaginous-only lesions, normal and abnormal cartilage can be differentiated on the basis of markedly lower T2* values in the core of the lesion, which likely represent necrotic epiphyseal cartilage, given similar T2* and histologically confirmed findings in animal studies (11). Histologic lesion patterns were identified as containing *(a)* cartilage alone and *(b)* laminar calcification and/or ossification (24,25). The laminar calcification and/or ossification pattern was found frequently in histologic studies of OCD plugs (26,27). The interface was described as fibrous, cartilaginous, osseous, cystic, or laminar, which suggests an entire spectrum of tissue response (24,25,27).

It is widely accepted that once a lesion is diagnosed, stability of the lesion in combination with the integrity of the overlying cartilage determines the

treatment strategy (eg, nonsurgical vs surgical treatment) and is an important predictor of outcome. However, current clinical MR imaging methods, even at this relatively late stage of disease, are disappointing when compared with the reference standard of arthroscopy (1,8,28–30). The management of JOCD in the knee remains highly controversial, largely owing to the paucity of high-quality studies (10,31,32). The additional information on lesion composition obtained with our imaging paradigm might be used to guide different treatment strategies, targeting solely cartilaginous versus secondarily ossified lesions.

Our pilot study has limitations, the most substantial of which is the small number of cases. Overall, JOCD is a rare disease and is typically advanced when patients present with classic clinical signs of pain. Therefore, it is extremely rare to identify early cartilage lesions. Ideally, these cases would also have arthroscopic correlations to validate the MR imaging findings. Although our study is not longitudinal, it does provide pictorial evidence of OCD lesion progression through several individual snapshots in time. More systematic and longitudinal studies in larger patient populations are needed to more thoroughly track the natural history of this disease process by using the suggested short-TE imaging approach. Another limitation is the lack of a control group. Images of normal knees were not acquired routinely, making the use of a contralateral knee as a control unfeasible. Additionally, the contralateral knee may not even serve well as a control, since about 30% of the disease occurs bilaterally (33). We based the decision to use the contralateral side (medial vs lateral epicondyle) as the appropriate control on the basis of prior studies in which the spatial variation of T2 values was measured in normal knees (34), which supports the notion that normal spatial variation of T2 and/or T2* between the medial and lateral femoral epicondyles is expected to be substantially smaller than the difference between normal and necrotic cartilage (11).

In conclusion, our modified MR imaging protocol allowed for identification of the epiphyseal cartilage origin and subsequent stages of ossification of JOCD, leading to important insights into the natural history of the disease by allowing differentiation of tissues that are otherwise hypointense and indistinguishable with current clinical imaging techniques. While JOCD has been previously defined as a localized process in which a focus of subchondral bone separates from the surrounding parent bone (35), our study demonstrated epiphyseal cartilage necrosis in the lesion, linking JOCD to failure of the articular-epiphyseal cartilage complex as described previously in animals (17). Furthermore, our observation of subsequent laminar marginal ossification that originates from the peripheral aspect of the lesion closest to the normally advancing ossification front has not been described before, to our knowledge.

References

1. Edmonds EW, Polousky J. A review of knowledge in osteochondritis dissecans: 123 years of minimal evolution from König to the ROCK study group. Clin Orthop Relat Res 2013;471(4):1118–1126.

2. König F. Über freie Körper in den Gelenken. Dtsch Z Chir 1887;27:90–109.

3. Chambers HG, Shea KG, Anderson AF, et al. American Academy of Orthopaedic Surgeons clinical practice guideline on: the diagnosis and treatment of osteochondritis dissecans. J Bone Joint Surg Am 2012;94(14):1322–1324.

4. Kocher MS, Micheli LJ, Yaniv M, Zurakowski D, Ames A, Adrignolo AA. Functional and radiographic outcome of juvenile osteochondritis dissecans of the knee treated with transarticular arthroscopic drilling. Am J Sports Med 2001;29(5):562–566.

5. Wall EJ, Polousky JD, Shea KG, et al. Novel radiographic feature classification of knee osteochondritis dissecans: a multicenter reliability study. Am J Sports Med 2015;43(2):303–309.

6. Brittberg M. ICRS Cartilage Evaluation Package. http://www.http://cartilage.org/wp-content/uploads/2014/10/ICRS_evaluation.pdf. Published 2000. Accessed August 6, 2002.

7. De Smet AA, Fisher DR, Graf BK, Lange RH. Osteochondritis dissecans of the knee: value of MR imaging in determining lesion stability and the presence of articular cartilage defects. AJR Am J Roentgenol 1990;155(3):549–553.

8. Kijowski R, Blankenbaker DG, Shinki K, Fine JP, Graf BK, De Smet AA. Juvenile versus adult osteochondritis dissecans of the knee: appropriate MR imaging criteria for instability. Radiology 2008;248(2):571–578.

9. Jacobs JC Jr, Archibald-Seiffer N, Grimm NL, Carey JL, Shea KG. A review of arthroscopic classification systems for osteochondritis dissecans of the knee. Orthop Clin North Am 2015;46(1):133–139.

10. Yellin JL, Gans I, Carey JL, Shea KG, Ganley TJ. The surgical management of osteochondritis dissecans of the knee in the skeletally immature: a survey of the Pediatric Orthopaedic Society of North America (POSNA) membership. J Pediatr Orthop 2015 Dec 2. [Epub ahead of print]

11. Wang L, Nissi MJ, Tóth F, et al. Multiparametric MRI of epiphyseal cartilage necrosis (osteochondrosis) with histological validation in a goat model. PLoS One 2015;10(10):e0140400.

12. Nissi MJ, Tóth F, Wang L, Carlson CS, Ellermann JM. Improved visualization of cartilage canals using quantitative susceptibility mapping. PLoS One 2015;10(7):e0132167.

13. Nissi MJ, Toth F, Zhang J, et al. Susceptibility weighted imaging of cartilage canals in porcine epiphyseal growth cartilage ex vivo and in vivo. Magn Reson Med 2014;71(6):2197–2205.

14. Tóth F, Nissi MJ, Zhang J, et al. Histological confirmation and biological significance of cartilage canals demonstrated using high field MRI in swine at predilection sites of osteochondrosis. J Orthop Res 2013;31(12):2006–2012.

15. Tóth F, Nissi MJ, Ellermann JM, et al. Novel application of magnetic resonance imaging demonstrates characteristic differences in vasculature at predilection sites of osteochondritis dissecans. Am J Sports Med 2015;43(10):2522–2527.

16. Laor T, Zbojniewicz AM, Eismann EA, Wall EJ. Juvenile osteochondritis dissecans: is it a growth disturbance of the secondary physis of the epiphysis? AJR Am J Roentgenol 2012;199(5):1121–1128.

17. Ytrehus B, Carlson CS, Ekman S. Etiology and pathogenesis of osteochondrosis. Vet Pathol 2007;44(4):429–448.

18. Olsson SE, Reiland S. The nature of osteochondrosis in animals. Summary and conclusions with comparative aspects on osteochondritis dissecans in man. Acta Radiol Suppl 1978;358:299–306.

19. Carlson CS, Hilley HD, Henrikson CK, Meuten DJ. The ultrastructure of osteochondrosis of the articular-epiphyseal cartilage complex in growing swine. Calcif Tissue Int 1986;38(1):44–51.

20. Blumer MJ, Longato S, Fritsch H. Structure, formation and role of cartilage canals in the developing bone. Ann Anat 2008;190(4):305–315.

21. Olstad K, Ytrehus B, Ekman S, Carlson CS, Dolvik NI. Early lesions of articular osteochondrosis in the distal femur of foals. Vet Pathol 2011;48(6):1165–1175.

22. Tóth F, Nissi MJ, Wang L, Ellermann JM, Carlson CS. Surgical induction, histological evaluation, and MRI identification of cartilage necrosis in the distal femur in goats to model early lesions of osteochondrosis. Osteoarthritis Cartilage 2015;23(2):300–307.

23. Chiroff RT, Cooke CP 3rd. Osteochondritis dissecans: a histologic and microradiographic analysis of surgically excised lesions. J Trauma 1975;15(8):689–696.

24. Yonetani Y, Nakamura N, Natsuume T, Shiozaki Y, Tanaka Y, Horibe S. Histological evaluation of juvenile osteochondritis dissecans of the knee: a case series. Knee Surg Sports Traumatol Arthrosc 2010;18(6):723–730.

25. Uozumi H, Sugita T, Aizawa T, Takahashi A, Ohnuma M, Itoi E. Histologic findings and possible causes of osteochondritis dissecans of the knee. Am J Sports Med 2009;37(10):2003–2008.

26. Zbojniewicz AM, Stringer KF, Laor T, Wall EJ. Juvenile osteochondritis dissecans: correlation between histopathology and MRI. AJR Am J Roentgenol 2015;205(1):W114–W123.

27. Barrie HJ. Hypertrophy and laminar calcification of cartilage in loose bodies as probable evidence of an ossification abnormality. J Pathol 1980;132(2):161–168.

28. Ellermann JM, Donald B, Rohr S, et al. Magnetic resonance imaging of osteochondritis dissecans: validation study for the ICRS classification system. Acad Radiol 2016;23(6):724–729.

29. Heywood CS, Benke MT, Brindle K, Fine KM. Correlation of magnetic resonance imaging to arthroscopic findings of stability in juvenile osteochondritis dissecans. Arthroscopy 2011;27(2):194–199.

30. Pascual-Garrido C, Moran CJ, Green DW, Cole BJ. Osteochondritis dissecans of the knee in children and adolescents. Curr Opin Pediatr 2013;25(1):46–51.

31. Carey JL, Grimm NL. Treatment algorithm for osteochondritis dissecans of the knee. Orthop Clin North Am 2015;46(1): 141–146.

32. LaPrade RF, Bursch LS, Olson EJ, Havlas V, Carlson CS. Histologic and immunohistochemical characteristics of failed articular cartilage resurfacing procedures for osteochondritis of the knee: a case series. Am J Sports Med 2008;36(2):360–368.

33. Cooper T, Boyles A, Samora WP, Klingele KE. Prevalence of bilateral JOCD of the knee and associated risk factors. J Pediatr Orthop 2015;35(5):507–510.

34. Hannila I, Räinä SS, Tervonen O, Ojala R, Nieminen MT. Topographical variation of T2 relaxation time in the young adult knee cartilage at 1.5 T. Osteoarthritis Cartilage 2009;17(12):1570–1575.

35. Grimm NL, Weiss JM, Kessler JI, Aoki SK. Osteochondritis dissecans of the knee: pathoanatomy, epidemiology, and diagnosis. Clin Sports Med 2014;33(2):181–188.